Contents lists available at ScienceDirect

Applied Catalysis B: Environmental

Improvement of photocatalytic and photoelectrochemical activity of ZnO/TiO₂ core/shell system through additional calcination: Insight into the mechanism

Maciej Kwiatkowski [a,b,*], Rémi Chassagnon [a], Olivier Heintz [a], Nicolas Geoffroy [a], Magdalena Skompska [b,c], Igor Bezverkhyy [a]

[a] Laboratoire Interdisciplinaire Carnot de Bourgogne, UMR 6303 CNRS-Université de Bourgogne Franche-Comté, 9 Avenue Alain Savary, BP 47870-21078, Dijon Cedex, France
[b] Laboratory of Electrochemistry, Faculty of Chemistry, University of Warsaw, Pasteur 1, 02-093 Warsaw, Poland
[c] Biological and Chemical Research Centre, Faculty of Chemistry, University of Warsaw, Zwirki i Wigury 101, 02-089 Warsaw, Poland

ARTICLE INFO

ABSTRACT

ZnO/TiO₂ composites were prepared by sol-gel deposition of TiO₂ on ZnO nanorods hydrothermally grown on electrically conductive indium tin oxide substrate (ITO). It has been shown that the ZnO/TiO₂ interface plays a key role in enhancement of photodecomposition of methylene blue (MB) used as a model test pollutant, under monochromatic light irradiation (400 nm). The increase of photocatalytic activity was attributed to the shift of absorption edge of ZnO/TiO₂ towards visible light in comparison with bare TiO₂. Further enhancement of photocatalytic activity of ZnO/TiO₂ was achieved through its additional calcination at 450 °C for 3 h. This treatment brings 40% increase in the rate of MB decomposition and a two-fold rise of the photocurrent in H₂O oxidation. Measurements of open circuit potential (V_{oc}) showed that the improved properties of additionally calcined ZnO/TiO₂ composites stem from decrease of the electron-hole recombination rate. Scanning transmission electron microscopy (STEM) studies showed that the additional calcination resulted in formation of voids at the ZnO/TiO₂ interface. Energy dispersive X-ray (EDX) and X-ray photoelectron (XPS) spectroscopies proved that formation of voids is accompanied by the outward diffusion of Zn ions into TiO₂ layer and allowed to conclude about the existence of the Kirkendall effect at ZnO/TiO₂ interface. Occurrence of this effect observed for the first time at such moderate temperature (450 °C) is attributed to a highly defective nature of the surface layer of the ZnO nanorods.

1. Introduction

Over the last 20 years, the interest in preparation and study of photo-active metal oxides has grown immensely. A great attention to these inorganic semiconducting materials has not been diminished since then [1–7], mostly due to not yet completely revealed and understood mechanisms that are responsible for improved photo-properties of such materials. Particularly, wide band gap (E_g) metal oxides, such as ZnO ($E_g \sim 3.3$ eV) [8], or TiO₂ ($E_g \sim 3.2$ eV) [9,10] are still among the most attractive base materials in the field of light-to-energy conversion. The advantages of ZnO and TiO₂ include relatively low cost, facile preparation, and stability under light irradiation. The main drawback of these materials is their poor efficiency under visible light due to the wide band gap. Several approaches have been proposed to overcome this problem such as doping with non-metal elements (N, S, B) [11–15], noble metal nanoparticle deposition (Au, Ag, Pt) [16–20] or by association with other semiconductors i.e. CdS [21,22], CdSe [23,24], or other transition metal oxides [25–27].

One of the ways being actively tested during recent years was the combination of ZnO and TiO₂ through the preparation of well-defined core-shell nanostructured composites in which either ZnO is deposited onto TiO₂ (TiO₂/ZnO) [28–30], or this is done in the reverse fashion (ZnO/TiO₂) [31–33]. Different techniques and methods were used to combine these oxides i.e. chemical vapor deposition (CVD) [34], atomic layer deposition (ALD) [35–39], radio-frequency magnetron sputtering [40], sol-gel approach [41,42], or by electrospun [43]. While the enhanced

photocatalytic and/or photoelectrochemical properties are still systematically reported for these composites [44–46], the role of some important preparation parameters has not yet been clarified. However, it is worth noting that the recent studies concluded that different gas atmosphere during heating of ZnO/TiO_2 composites prepared by sol-gel method result in improvement of photocatalytic and photoelectrochemical properties [47]. Likewise, appropriately designed and fabricated microstructure may also result in a significant increase of water-splitting efficiency at the ZnO/TiO_2 composite photoelectrodes [48]. Also, recently it has been reported that a rapid cooling process after calcination caused a thermal stress in ZnO/TiO_2 nanostructures and ultimately proved to increase photocatalytic activity of the composite [49]. Additionally, in our previous work we have found that the higher rate of photocatalytic degradation of methylene blue (MB) was achieved for the ZnO/TiO_2 core-shell composites prepared via sol-gel synthesis with better accessibility to the ZnO/TiO_2 interface [50].

In the present study we provide the first evidence that additional calcination of the ZnO/TiO_2 composite at 450 °C modifies the interface between the two oxides leading to significant improvement of decolorization rate of MB and photoassisted decomposition of H_2O under 400 nm monochromatic irradiation. The changes at the boundary between ZnO and TiO_2 upon additional calcination were evidenced by HAADF-STEM and XPS and the mechanism of interfacial transformation is discussed.

2. Experimental

2.1. Materials

All chemicals including: Titanium(IV) butoxide (97%), 2-propanol ($\geq$99.9%), $Zn(NO_3)_2 \cdot 6H_2O$ ($\geq$99%), $Zn(CH_3COO)_2 \cdot 2H_2O$ ($\geq$99.5%), $HCl_{(aq.)}$ (37%, Rotipuran), Na_2SO_4 ($\geq$99%), KCl ($\geq$99%), $NH_3 \cdot H_2O$ ($\geq$23%), methylene blue ($C_{16}H_{18}N_3SCl$, $\geq$95%) were provided by ROTH or Sigma-Aldrich, and were used as received without further purification. Deionized water (Millipore, 18 MΩ cm) was used to prepare aqueous solutions. Indium Tin Oxide (ITO) conducting glass support of a sheet resistance 20 $\Omega\square^{-1}$ was purchased from Prazisions Glass & Optik GmbH (Germany).
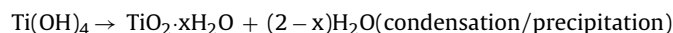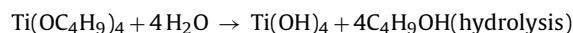
2.2. Preparation of ZnO nanorods

ZnO nanorods were deposited on ITO surface according to the procedure reported in our earlier paper [51]. Prior to deposition, the ITO plates were cleaned by sequential immersion for 15 s in 3 M NaOH, deionized water and concentrated H_2SO_4. Then, the ITO substrates were seeded with nanostructural Zn (in the form of blocks and nanosheets) by potentiostatic deposition at −1.2 V vs. Ag/AgCl/Cl$^-$ (3 M) reference electrode, with a Pt wire as the counter electrode, in non-deareated aqueous solution of 0.1 M $Zn(CH_3COO)_2$. Then, the plates were annealed in air at 300 °C for 1 h to transform the superficial layer of Zn into ZnO. A hydrothermal synthesis of ZnO nanostructures on the seeded ITO substrates was performed from 0.04 M $Zn(NO_3)_2$ aqueous solution at fixed pH 10.6, in tightly closed Teflon® reactor at 80 °C. After 2.5 h, the reactor was quickly cooled down to ambient temperature. The samples were washed thoroughly with deionized water and calcined at 300 °C for 1 h (hereafter, *ZnO-plates*).

2.3. Preparation of ZnO/TiO_2 core-shell systems and their thermal modification

ZnO/TiO_2 composites were prepared via sol-gel deposition method described in detail elsewhere [50]. *ZnO-plates* (with ZnO grown only on the seeded substrate of the surface area of 1.5 cm^2)

were placed upside-down in isopropanol containing TiO_2 precursor, titanium(IV) butoxide (*TIB*) in a volume ratio 100:1, in an open glass reactor at ambient temperature. After 15 min of conditioning, a portion of water was slowly introduced (H_2O:*TIB* molar ratio of was 4:1) in order to initiate hydrolysis of *TIB* followed by condensation/precipitation according to the reaction schemes:

$$Ti(OC_4H_9)_4 + 4 H_2O \rightarrow Ti(OH)_4 + 4C_4H_9OH (hydrolysis)$$

$$Ti(OH)_4 \rightarrow TiO_2 \cdot xH_2O + (2 - x)H_2O (condensation/precipitation)$$

After 30 min, the samples were gently washed with 2-propanol and ethanol, dried in air and calcined at 450 °C for 1 h to transform the layer of amorphous TiO_2 deposited on ZnO nanorods into TiO_2-anatase phase. Upside-down arrangement of the *ZnO-plates* during synthesis allowed to avoid formation of undesirable over-layers of deposit on the nanorods. The whole procedure was accomplished 3-times to obtain final ZnO/TiO_2 core-shell composites (denoted as "**ZT**"). In order to modify initial ZnO/TiO_2 composites (**ZT**) the samples were additionally calcined for 3 h at 450 °C ("**ZT-Cal**").

In some experiments **ZT** and **ZT-Cal** samples were treated by immersing into HCl aqueous solution of pH 3 for 20 h in order to remove ZnO cores to obtain finally "**ZT-HCl**", and "**ZT-Cal-HCl**", named respectively. SEM and TEM images of samples with dissolved ZnO-cores can be found in Appendix Supplementary information (Fig. A1).

2.4. Characterization and methods

Morphology was investigated by scanning electron microscopy (SEM, JEOL-7600F). Internal microstructures were studied by a transmission electron microscopy using high-angle annular dark-field scanning transmission electron microscopy mode (HAADF-STEM, JEOL JEM-2100 F 200 kV). X-ray Photoelectron spectroscopy (XPS) was applied in order to determinate atomic states and surface composition of samples by usage of apparatus PHI 5000 Versaprobe with mono-chromatic Al Kα1 X-Rays. XRD measurements were carried out in the range of 2-theta angle 20°–70° with a diffractometer Bruker D8-A25 Discover fitted with a LynxEyeXE detector. The photoluminescence emission spectra of the samples were recorded using Fluorolog-3 spectrofluorometer (Horiba Scientific) with a 400 nm excitation wavelength at room temperature. Optical properties of the samples were determined from UV–vis spectra recorded in the wavelength range 300 nm–700 nm by means of Shimadzu UV-2550 spectrophotometer equipped with integration sphere. The same spectrophotometer was used for transmission photometric studies of decolorization of methylene blue (MB), used as a model pollutant (ISO 10678-2010) for evaluation of the material photocatalytic properties [52]. The photocatalysts immersed in MB solution of initial concentration 10 mM were irradiated with monochromatic light of 400 nm emitted by a high-power LED (140 mW cm^{-2}, provided by LED Engin, USA), according to the procedure described elsewhere [34]. The change of MB concentration was determined from decrease of absorbance maximum intensity in the UV–vis spectrum at the wavelength of 664 nm. Decomposition of MB obeys the first-order kinetics and an apparent first-order rate constant was determined from the linear slope of the plot of logarithm of concentration ratio (C/C_o) as a function of time. Prior to photodecomposition studies each sample was kept in 20 mM aqueous solutions of MB for 24 h to avoid concentration drop due to dye adsorption on the metal oxide during the photocatalytic test.

The (photo)electrochemical experiments were performed in three electrode cell, with ITO/ZnO/TiO_2 as working electrode, a Pt wire as counter electrode and aqueous Ag/AgCl/Cl$^-$ (3 M) as reference electrode. The linear sweep voltammograms (LSV),
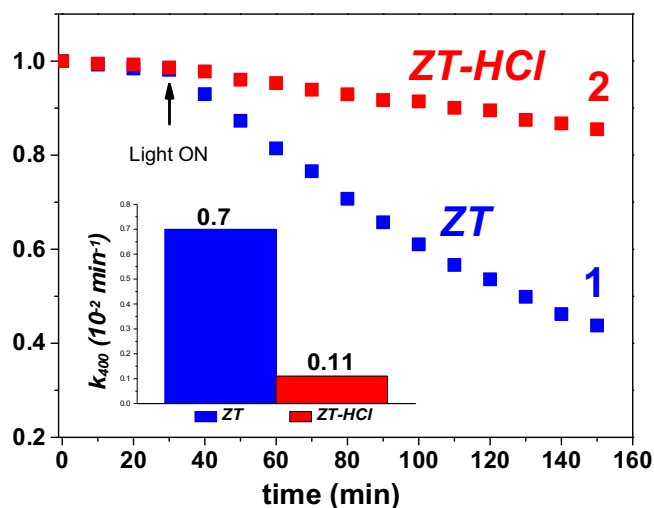
Fig. 1. Photodegradation of MB with the use of the ZnO/TiO$_2$ composites before (blue scatter 1, *ZT*) and after dissolution (red scatter 2, *ZT-HCl*) of ZnO cores in HCl (A). Inset: values of pseudo first-order rate constants (k_{400}) calculated for *ZT* (blue) and *ZT-HCl* (red). (For interpretation of the references to colour in this figure legend, the reader is referred to the web version of this article.)

Fig. 2. Absorption spectra of *ZT* (blue curve 1), *ZT-HCl* (red curve 2), whereas the black curve 3 corresponds to the spectrum obtained for TiO$_2$. (For interpretation of the references to colour in this figure legend, the reader is referred to the web version of this article.)

chronoamperograms and open circuit potential decay measurements (V_{oc}) were performed by means of potentiostat Autolab (Metrohm B. V., The Netherlands). The working electrode of the surface area of about 1 cm^2 was illuminated, as in photocatalytic tests, with monochromatic light of the wavelength of 400 nm. The V_{oc} experiments were carried out in deareated aqueous solution of 0.2 M KCl in phosphate buffer of pH 6.8, while the LSV with the scan rate of 10 mV s^{-1} and chronoamperometric measurements at the potential of 0.8 V were performed in aqueous solution of 5 mM Na$_2$SO$_4$.

3. Results and discussion

3.1. Evidence for a key role of ZnO/TiO$_2$ interface in photocatalysis

Importance of the ZnO/TiO$_2$ interface in the photocatalytic degradation of MB was proved by comparative studies performed in the presence of the *ZT* sample and the sample after dissolution of the ZnO cores in HCl$_{(aq.)}$ of pH 3 for 20 h (*ZT-HCl*). The results presented in Fig. 1 indicate that decolorization rate of MB significantly decreased after treatment of *ZT* photocatalyst with HCl and
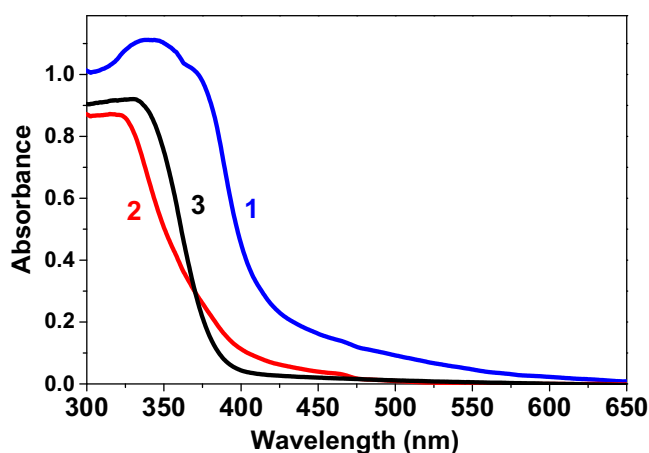
the apparent rate constant of the process (k_{400}) deteriorated by a factor of 6.4 with respect to that obtained for the standard the *ZT* sample. These results show that the presence of ZnO/TiO$_2$ interface plays indeed a crucial role in the photocatalytic process. In order to understand the origin of this effect the diffuse reflectance spectra of the samples were recorded.

The UV–vis spectrum of the *ZT* sample (curve 1 in Fig. 2) presents two characteristic features: formation of a pronounced "Urbach tail" in the wavelengths range from 600 nm to 420 nm, absent in the spectrum of TiO$_2$ powder, and the shift of the absorption threshold towards visible range. Consequently, these two effects may be ascribed to the formation of interfacial states at the ZnO/TiO$_2$ boundary, with the energy levels localized in the band gap [53]. As a result, the sub-band gap optical transitions become possible. However, the treatment of the sample with HCl$_{(aq.)}$ leads to the shift of the spectrum back towards UV range and to significant diminution of the absorbance tail. This behavior may be explained by disappearance of the interfacial states due to removal of ZnO in HCl$_{(aq.)}$. Since the results presented above supported the key role of ZnO/TiO$_2$ interface in photocatalytic activity of the composite, an attempt to modify the interfacial region was undertaken through additional calcination. The samples prepared by the standard procedure were submitted to additional calcination for 3 h at
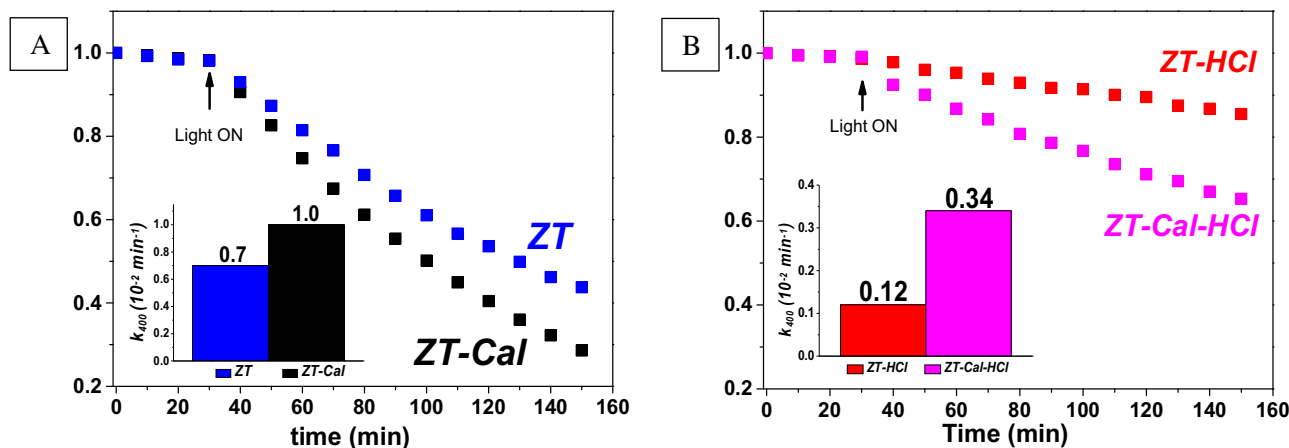

Fig. 3. (A) Photodecomposition of MB on the catalysts: *ZT* (initial sample), *ZT-Cal* (*ZT* additionally calcined). (B) *ZT-HCl* (*ZT* after HCl-treatment), and *ZT-Cal-HCl* (*ZT* additionally calcined with subsequent HCl-treatment).
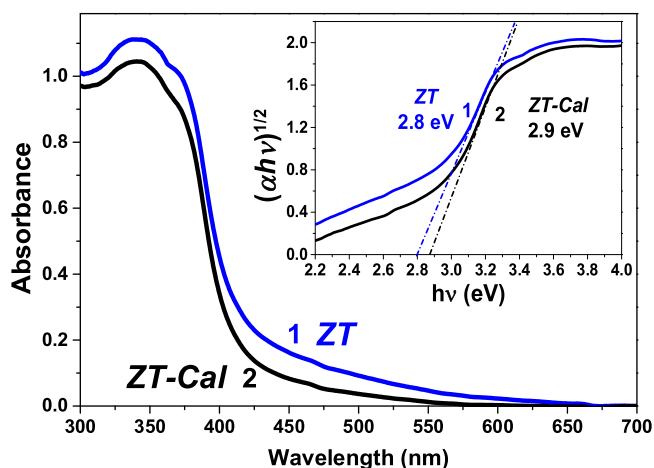
Fig. 4. Optical properties of the ZnO/TiO₂ composites: initial **ZT** sample (1, blue curves), and after additional calcination **ZT-Cal** (2, black curves). Inset: the Tauc plots used for determination of optical band gaps (E_g) of the samples. (For interpretation of the references to colour in this figure legend, the reader is referred to the web version of this article.)

Fig. 5. Open-circuit potential (V_{oc}) decay after switching off the light for the **ZT** (1) and **ZT-Cal** (2) samples. The V_{oc} measurements were recorded in deareated aqueous solution of 0.2 M KCl in phosphate buffer of pH 6.8. Inset 5: the plots of lifetime (τ_e) of the photogenerated charge carriers, derived from Eq. (1) as a function of V_{oc} for **ZT** and **ZT-Cal**.

450 °C (**ZT-Cal**) and then were treated as before in HCl solution (**ZT-Cal-HCl**).

The results of MB photocatalytic degradation (Fig. 3A) show that additional calcination leads to the increase of activity of the ZnO/TiO₂ composite (the apparent first-order rate constant increases from $k'_{400} = 0.7 \times 10^{-2}\,min^{-1}$ for **ZT**, to $k''_{400} = 1.0 \times 10^{-2}\,min^{-1}$ for **ZT-Cal**). It is also interesting to note that the photocatalytic activity of the composite additionally calcined before ZnO dissolution (**ZT-Cal-HCl**) is remarkably higher (almost 3-times) than that of **ZT-HCl** (Fig. 3B).

The results presented above suggest that additional calcination significantly modifies the interfacial ZnO/TiO₂ region and thus influences the photocatalytic activity of the composites. Improvement of the activity by a simple additional calcination is an interesting result and we tried to understand the origin of this enhancement.

3.2. Explanation of the improved properties of additionally calcined ZnO/TiO₂

First, we supposed that it stems from the decrease of the optical band gap and therefore, better absorption in visible range after
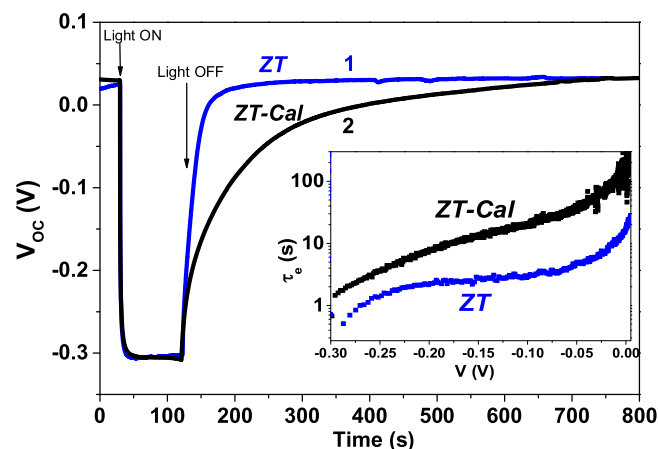
additional calcination. As visible in Fig. 4, the spectrum of **ZT-Cal** slightly differs from **ZT** in the visible range, between 420 nm and 600 nm. The calcination leads to diminishing of the "Urbach tail" and decrease of the absorbance in this range. The Tauc plots [54] (inset, Fig. 4) indicate that additional calcination leads to a small increase of the optical band gap, from 2.8 eV for **ZT** to 2.9 eV for **ZT-Cal**. However, the absorbance at 400 nm (at which the photocatalytic tests were performed) of **ZT-Cal** sample is very similar to that of **ZT**. Thus, the modification of the optical properties can hardly explain the observed increase of catalytic activity. The similarity of the optical properties of **ZT** and **ZT-Cal** samples at 400 nm means that the number of generated electron-holes pairs is similar in both cases.

In these conditions the higher activity of **ZT-Cal** might be related to a lower electron-hole recombination rate in this sample. To check this possibility the composites were characterized by photoelectrochemical measurements of open-circuit potential (V_{oc}) decay. The **ZT** and **ZT-Cal** samples were illuminated with light of the wavelength 400 nm for 90 s and then the light was turned off and relaxation of the open circuit potential was monitored within 680 s. The V_{oc} results presented in Fig. 5 show that both samples exhibit very similar behavior under illumination and open circuit potential reach the value of −300 mV (time range 30 s–120 s). Also, both
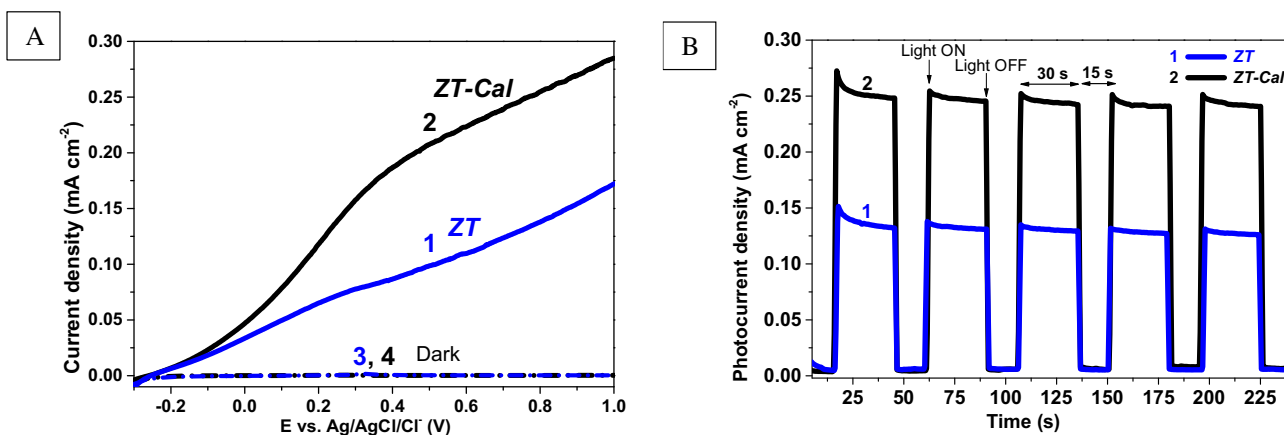

Fig. 6. (A) Linear sweep voltammograms for the **ZT** (blue curves, 1 and 3) and **ZT-Cal** (black curves, 2 and 4) electrodes in dark (dash-dotted curves) and under illumination (solid curves). LSV taken at a sweep rate of 10 mV s⁻¹ in 5 mM Na₂SO₄ aqueous solution, while the photocurrent transients (B) of **ZT** (blue, 1) and **ZT-Cal** (black, 2) were measured at constant potential of 0.8 V vs. $E_{Ag/AgCl/Cl^-}$. (For interpretation of the references to colour in this figure legend, the reader is referred to the web version of this article.)

samples showed typical behavior during light-off relaxation (time range 120 s–800 s) for TiO_2-based electrodes, as reported in the literature [55,56], However, a significant difference between **ZT** and **ZT-Cal** was observed in the course of V_{oc} transients during light-off relaxation from the illuminated state to the dark equilibrium.

In the case of the **ZT** sample, the initial dark value of V_{oc} was reached within 120 s, whereas the relaxation time was much longer (~700 s) for the **ZT-Cal**. These results confirm our hypothesis that photogenerated electrons in the samples differ in recombination lifetimes. For ZnO, and TiO_2 the results of V_{oc} decay can be used to estimate electron recombination lifetime, [57] accordingly to the eq.: [58]

$$\tau_e = -\frac{kT}{e}\left(\frac{dV_{OC}}{dt}\right)^{-1} \qquad (1)$$

where k stands for the Boltzmann constant, e for the elementary charge and T is the temperature expressed in Kelvins. Inset in Fig. 5 shows that indeed in the **ZT-Cal** sample the electron-hole pair recombination process is longer than that in the initial **ZT** sample. These results allow to ascribe the improved photocatalytic activity of the additionally calcined sample to the prolonged photoelectron and hole lifetime. Thus the photogenerated charge carriers can be more efficiently utilized in the decomposition of MB.

In order to examine how the hindered electron-hole recombination in the **ZT-Cal** composite influences the photoelectrochemical properties of the system, the investigation of both samples (**ZT** and **ZT-Cal**) in dark and under illumination was performed by linear sweep voltammetry and chronoamperometry. As visible in Fig. 6A, 2-times higher photocurrent was obtained for the **ZT-Cal** electrode than that for the **ZT** sample, in a broad range of applied potentials (from 0.4 V to 1.0 V) under illumination at 400 nm (solid curves 1 and 2), whereas the dark currents for both samples were negligible (dash-dotted curves 3 and 4). The appearance of anodic photocurrent means that the photogenerated holes from valence band take part in oxidation of the surface $Ti-O^-$ groups to $Ti-O^\bullet$ radicals and/or adsorbed hydroxyl groups to $^\bullet OH$ radicals [59], as well as in photo-assisted water oxidation [60]. At the same time the electrons from CB are transported to the ITO substrate and then to the external circuit. The significant increase of photocurrent upon additional calcination can be explained, as in the case of V_{oc} by prolonged lifetime of the photogenerated charge carriers and increased flux of the electrons to the external circuit. The same conclusions may be derived from the photocurrent transients recorded at constant potential of 0.8 V vs Ag/AgCl/Cl$^-$, presented in Fig. 6B, where the photocurrent is almost two times higher for the additionally calcined sample. It is also important to note that after illumination of the electrode the photocurrent stabilizes within several seconds and the response is reproducible in the successive dark and illumination cycles.

Such strong positive effect of calcination on the photocatalytic and photoelectrochemical properties of the ZnO/TiO_2 system can be a result of morphological changes, especially at the interface. In order to verify this point we characterized the structural changes occurring during calcination. To this end, XPS and STEM with EDX elemental mapping and line scans were used. The obtained results are described in the next section.

3.3. Morphology and structure analysis

HAADF-STEM was used to examine thermal modifications of the ZnO/TiO_2 composites. By means of HAADF-STEM technique it is possible to acquire images in which the signal is proportional not only to the thickness but also to atomic number of the elements (Z-contrast). In the HAADF-STEM images presented in Fig. 7, the external TiO_2 shell, the ZnO core and so the internal structure of the composites can be clearly distinguished. The results for ZnO
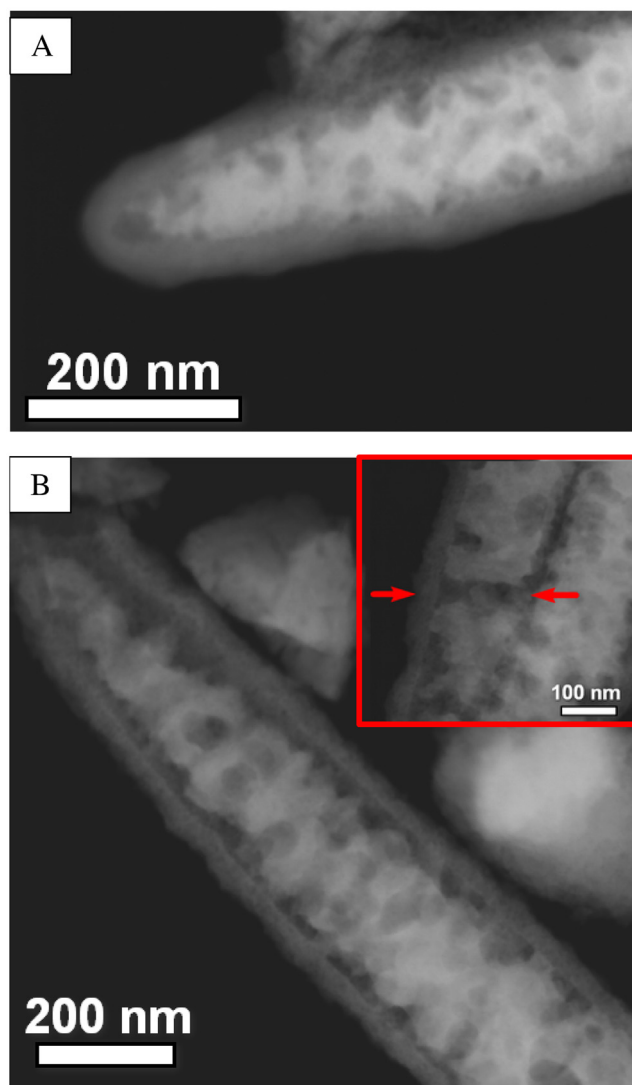

Fig. 7. HAADF-STEM images of ZnO/TiO_2 composites: **ZT** (A) and **ZT-Cal** (B). Inset in red frame shows a hollow channel through the **ZT-Cal** nanorod. (For interpretation of the references to colour in this figure legend, the reader is referred to the web version of this article.)

nanorods covered with as-deposited amorphous TiO_2 layer are presented in Fig. A2 (Appendix). Calcination of the sample for 1 h at 450 °C after each deposition cycle (in the **ZT** sample) gives rise to appearance of void spaces observed at the ZnO/TiO_2 interface. It is worth noting that additional calcination (3 h at 450 °C) provokes formation of bigger voids at the boundary between ZnO and TiO_2 (Fig. 7B). At a close inspection, it can be seen that the thickness of the external TiO_2 layer was not changed (~35 nm) after additional calcination, whereas the remaining ZnO-core appeared to be significantly "etched". The hollow spaces in the ZnO-core may even form void channels across the nanorod, as illustrated in the inset in Fig. 7B. The appearance of voids at the interface between two materials is an indication of the Kirkendall effect [61–64]. This effect consists in a more rapid diffusion of one of the components during solid-solid reaction. Such preferential diffusion of one solid (ZnO in our case) would lead to formation of voids at the interface between two solids. This effect should also result in enrichment of TiO_2 with Zn. To verify this fact EDX and XPS studies were carried out.

EDX-STEM atomic mapping and line scans of atomic profiles of the ZnO/TiO_2 systems were acquired to confirm the presence of
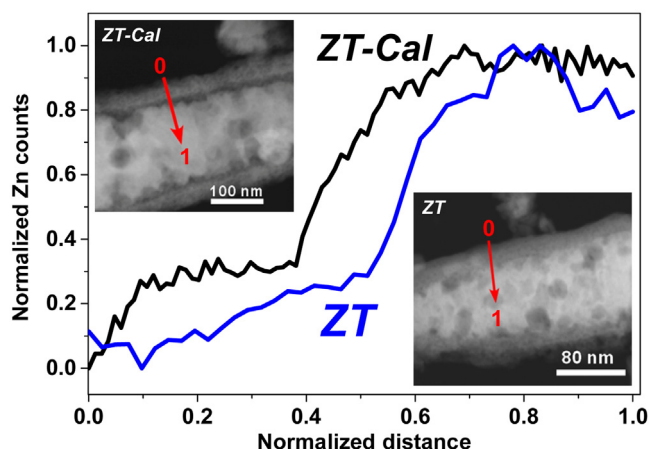
Fig. 8. Zinc concentration profiles obtained from linear EDX-STEM analysis across the ZnO/TiO$_2$ nanorod of **ZT** and **ZT-Cal**. Insets: HAADF-STEM images of the **ZT** (bottom) and **ZT-Cal** (top) samples with arrows indicating the line scan direction.
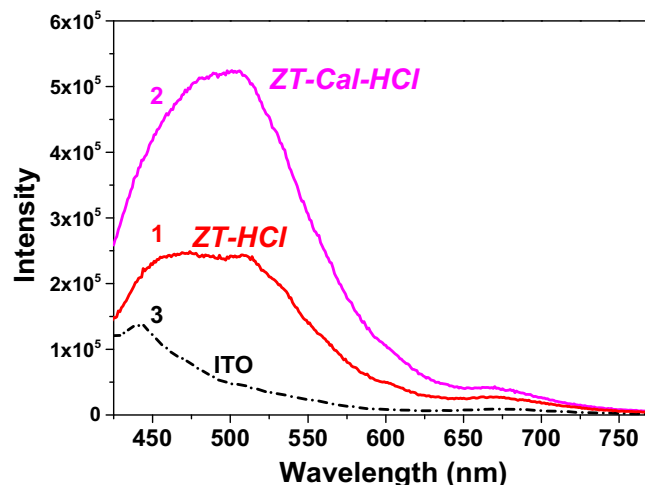

Fig. 9. Room-temperature photoluminescence spectra of **ZT-HCl** (1), **ZT-Cal-HCl** (2), and an ITO-support as reference (3), excited at 400 nm.

zinc in the TiO$_2$ external layer. The maps of elements distribution (Appendix, Fig. A3) indicate that zinc is indeed present in the TiO$_2$ layers of the **ZT** and **ZT-Cal** samples, before and after additional calcination. EDX-STEM line scan analyses were done along the red lines indicated in the images in Fig. 8. As visible, the amount of zinc increases in the outer part of TiO$_2$ layer after additional calcination of **ZT**. These results showed that the process of Zn ions diffusion into the TiO$_2$ layer takes place already in the **ZT** sample and becomes more pronounced after additional calcination in **ZT-Cal**.

To confirm the results of EDX analysis, the XPS spectra were measured for the **ZT**, **ZT-HCl**, **ZT-Cal**, and **ZT-Cal-HCl** samples (Appendix, Fig. A4). In the XPS spectra of all samples, the position of main Ti (2p$_{1/2}$) signal corresponds to TiO$_2$, the Zn (2p$_{3/2}$) signal to ZnO, and the O (1s) signals corresponds to O^{2-} in the lattice of metal oxides and hydroxyl groups [65,66]. The Zn:Ti atomic ratios calculated from the XPS spectra are given in Table 1. The Zn amount in the external layer increases significantly by factor of 2.7 when the **ZT** sample is additionally calcined (**ZT-Cal**). The same tendency is observed for **ZT-HCl** and **ZT-Cal-HCl** (factor of increase: 1.8). These results thus confirm that the formation of voids is accompanied by Zn^{2+} diffusion into the TiO$_2$ layer. Also, STEM images and XPS results ensure that the zinc signal was detected from Zn-modified most external parts TiO$_2$ layer and not from ZnO-core, due to porosity of TiO$_2$ layer. The data listed in Table 1 also show that the increase of the Zn/Ti ratio in the outer layer is nicely correlated with the increase of photocatalytic activity of the sample.

The conclusion about the enrichment of TiO$_2$ with zinc brings a question about the nature of the thus formed phase. It should be noted that a gradient of Zn concentration exists across the TiO$_2$ layer and consequently different phases might form depending on the distance from ZnO surface. Thus, zinc-rich titanates (Zn$_2$TiO$_4$ or ZnTiO$_3$) can exist in the close proximity to ZnO. In contrast, the bulk of TiO$_2$ layer can accommodate Zn ions in the form of a zinc-poor solid solution. The absence of any peak of zinc titanates in the

diffractograms of **ZT-Cal** (Appendix, Fig. A5) does not exclude their formation but indicates that the main phase is a zinc-containing TiO$_2$-anatase. This fact allows to propose the possible reason of the increase of the electron lifetime observed in the **ZT-Cal** material. We attribute it to the presence of oxygen vacancies whose formation allows to compensate the charge of Zn^{2+} cations incorporated into the TiO$_2$-anatase structure. Higher concentration of the oxygen vacancies in the Zn-doped TiO$_2$ is confirmed by the photoluminescence (PL) spectra of **ZT-HCl** and **ZT-Cal-HCl** (Fig. 9). The intensity of the peak at 510 nm, whose appearance was previously correlated with formation of oxygen vacancies [67–69], increases after additional calcination.

The influence of oxygen vacancies on the photocatalytic properties of TiO$_2$ is a subject of debates. While some studies suggest a negative role of these defects, other works describe enhanced properties of the defective samples [70]. This controversy is certainly due to a large number of parameters describing oxygen vacancies which are difficult to determine. Thus, their concentration, charge, spatial distribution, presence or absence of other species in their surrounding can all determine the way how the oxygen vacancies impact the photocatalytic properties of TiO$_2$. These parameters appear to be favorable in our case for decreasing the electron-hole recombination rate and consequently for improving photocatalytic and photoelectrochemical properties of the composite.

Our findings about modification of TiO$_2$ layer in the calcined composite allow to explain the stronger variation of the catalytic activity in MB decolorization observed in the etched samples (0.12×10^{-3} min^{-1} for **ZT-HCl** vs. 0.34×10^{-3} min^{-1} for **ZT-Cal-HCl**) than for the composite ones (7×10^{-3} min^{-1} for **ZT** vs. 10^{-2} min^{-1} for **ZT-Cal**).

We have shown previously [51] that high photocatalytic activity of ZnO/TiO$_2$ composites under 400 nm illumination was achieved due to appearance of two effects: i) formation of additional energy levels within the bandgap (allowing the sub-band optical transitions) and ii) enhancement of the separation efficiency of photogenerated e-h pairs. In the present study we found that additional calcination of ZnO/TiO$_2$ composite brings up the third effect – the increase of charge carriers lifetime. The first and the second effects were hence acting already in the pristine **ZT** sample due to the presence of ZnO/TiO$_2$ interface. The increase of the lifetime of the charge carriers appearing in **ZT-Cal** sample seems to be of a lower importance than two other effects and therefore, it does not lead to a dramatic increase of its photocatalytic activity in comparison with that of **ZT** sample. In contrast, in the etched samples

Table 1
The Zn:Ti ratios determined from the XPS spectra of initial **ZT** composite, **ZT** composite after additional calcination (**ZT-Cal**), and after HCl-treatment (**ZT-HCl**, **ZT-Cal-HCl**) and values of apparent first-order rate constant (k_{400}) of MB decomposition.

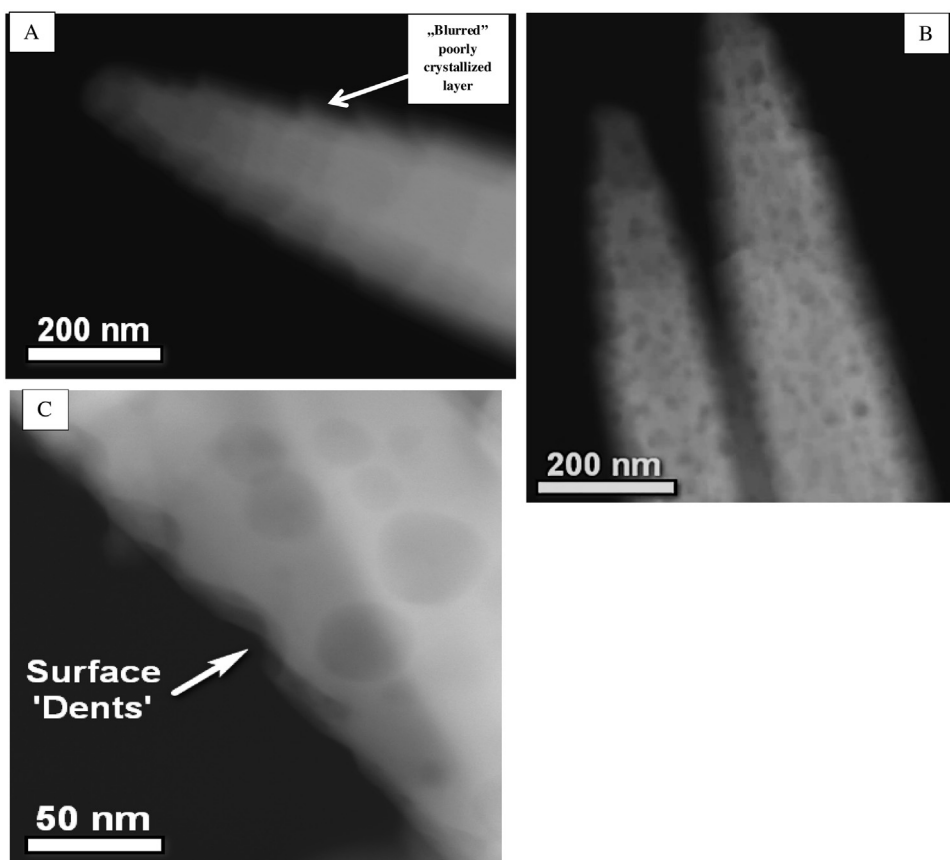| Sample	XPS Zn:Ti At.%	XPS Zn:Ti Ratio	MB decomposition rate constant k_{400} (10^{-2} min^{-1})
ZT	10:20	0.50	0.7
ZT-Cal	20.7:15.6	1.33	1.0
ZT-HCl	4.7:21.8	0.22	0.12
ZT-Cal-HCl	8.1:20.4	0.40	0.34

Fig. 10. HAADF-STEM images of as-synthesized ZnO sample (A), after calcination at different temperatures: 300 °C (B), and 450 °C (C).

(**ZT-HCl** and **ZT-Cal-HCl**) the ZnO/TiO$_2$ interface was eliminated and therefore, the related interfacial effects are no longer valid. The only difference between these two samples is a slower electron-hole recombination in **ZT-Cal-HCl** due to the presence of oxygen vacancies formed upon incorporation of Zn cations into TiO$_2$. This effect, although "masked" in the composites, becomes an essential one in the etched samples. This explains why the relative increase of the rate constant upon additional calcination is much larger in the HCl-etched samples than in the non-treated ones.

Migration of Zn ions into TiO$_2$ layer proceeds in our composite at 450 °C which is unusually low temperature for such phenomenon. Thus, in a very similar nanostructured ZnO-(core)-TiO$_2$-(shell) system the reaction proceeded at 700 °C [71]. We supposed that the higher reactivity of ZnO in our case is due to some particular properties of the surface layer of ZnO nanorods which is in direct contact with the TiO$_2$ shell. To clarify this point the surface microstructure of as-grown and calcined ZnO nanorods was characterized by HAADF-STEM.

3.4. Origin of the modification of the ZnO/TiO$_2$ interface at moderate temperature

Results of HAADF-STEM imaging of as-synthetized ZnO nanorods, the same nanorods after calcination at 300 °C, and ZnO nanorods calcined at 450 °C are presented in Fig. 10A, B and C respectively. It can be seen that ZnO nanorods after calcination at 300 °C contain numerous small dark spots on its surface. These extended surface defects designated as "dents" can be clearly disclosed on the HAADF-STEM image of ZnO nanorod calcined at higher temperature (450 °C, Fig. 10C). We speculate that these defects may be formed during crystallization of external amorphous layer of zinc (oxo)hydroxide obtained in hydrothermal

synthesis which can be seen as blurred external layer in Fig. 10A. Crystallization of this layer during calcination at 300 °C results in its shrinking and formation of a "dented" surface layer. Such rough surface should be enriched with steps and/or kinks which contain an important number of low coordinated Zn^{2+} possessing high reactivity. During sol-gel deposition the amorphous Ti-containing species fill up the "dents" at the ZnO surface and thus come in a close contact with the highly reactive Zn species. This particular configuration would allow for diffusion of Zn^{2+} into TiO$_2$ already at 450 °C. We consider thus that both the surface roughness of ZnO nanorods and the used sol-gel deposition method make possible Zn ion diffusion at such moderate temperature. A scheme depicting this possible diffusion scenario is presented in Fig. 11.
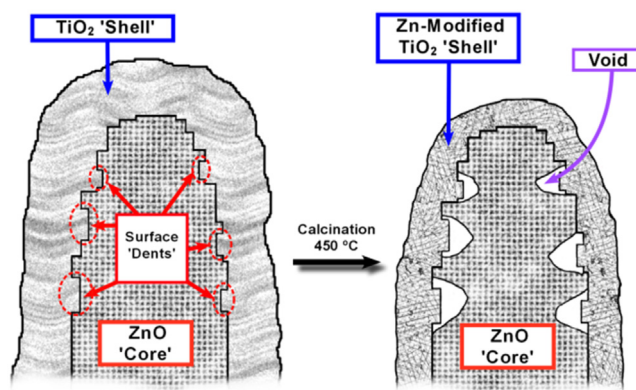

Fig. 11. A schematic illustration depicting presumable thermal diffusion process of Zn ions into TiO$_2$ at the ZnO/TiO$_2$ interface at 450 °C accompanied with formation of 'voids' in ZnO-core.

Hence, improved photocatalytic and photoelectrochemical properties of ZnO/TiO_2 composite can be attributed to the presence of ZnO/TiO_2 interface responsible for improved light absorption and to Zn-modified TiO_2 layers responsible for prolonged electron-hole pair recombination lifetime.

4. Conclusions

In this work it was proven that association of ZnO core with TiO_2 shell allows obtaining photoactive composites, which efficiently decompose a model pollutant: methylene blue (ISO 10678-2010) under 400 nm light irradiation. The origin of this effectiveness was shown to emerge from improved absorption in the visible range possibly due to formation of new electronic states at the ZnO/TiO_2 interface. Moreover, we found that an additional calcination of the ZnO/TiO_2 composite at 450 °C leads to the increase of photocatalytic activity in MB decomposition and remarkable improvement of the photocurrent response of the composite in photoassisted water splitting. The measurements of open circuit potential transients showed that this effect stems from a lower electron-hole recombination rate in the additionally calcined composite. The observed improvement of the photocatalytic properties was found to be accompanied by a pronounced modification of the microstructure of the ZnO/TiO_2 composite. Despite a moderate value of the used temperature (450 °C), voids appear at ZnO/TiO_2 interface and Zn ions migrate into TiO_2 shell. We suggest that formation of the Zn-enriched TiO_2 shell is responsible for the observed enhancement of the photocatalytic and photoelectrochemical properties. This phenomenon was ascribed to the Kirkendall effect which was observed for the first time at such low temperature due to defective surface structure of ZnO nanorods. Given the importance of ZnO and TiO_2 in photocatalysis these findings may be useful in designing more efficient photoactive materials, as well as in application of ZnO/TiO_2 composites in degradation of other pollutants.

Acknowledgements

Appendix A. Supplementary data

Supplementary data associated with this article can be found, in the online version, at http://dx.doi.org/10.1016/j.apcatb.2016.11.030.

References

[1] K. Rajeshwar, Solar energy conversion and environmental remediation using inorganic semiconductor–liquid interfaces: the road traveled and the way forward, J. Phys. Chem. Lett. 2 (2011) 1301–1309.

[2] P.V. Kamat, Quantum dot solar cells. The next big thing in photovoltaics, J. Phys. Chem. Lett. 4 (2013) 908–918.

[3] D. Fattakhova-Rohlfing, A. Zaleska, T. Bein, Three-dimensional titanium dioxide nanomaterials, Chem. Rev. 114 (2014) 9487–9558.

[4] F.E. Osterloh, Inorganic nanostructures for photoelectrochemical and photocatalytic water splitting, Chem. Soc. Rev. 42 (2013) 2294.

[5] S.G. Kumar, K.S.R. Koteswara Rao, Zinc oxide based photocatalysis: tailoring surface-bulk structure and related interfacial charge carrier dynamics for better environmental applications, RSC Adv. 5 (2015) 3306.

[6] Y. Wang, Q. Wang, X. Zhan, F. Wang, M. Safdar, J. He, Visible light driven type II heterostructures and their enhanced photocatalysis properties: a review, Nanoscale 5 (2013) 8326.

[7] J. Li, N. Wu, Semiconductor-based photocatalysts and photoelectrochemical cells for solar fuel generation: a review, Catal. Sci. Technol. 5 (2015) 1360.

[8] Ü. Özgür, Y.I. Alivov, C. Liu, A. Teke, M.A. Reshchikov, S. Doğan, V. Avrutin, S.-J. Cho, H. Morkoçd, A comprehensive review of ZnO materials and devices, J. Appl. Phys. 98 (2005) 041301.

[9] S. Banerjee, S.C. Pillai, P. Falaras, K.E. O'shea, J.A. Byrne, D.D. Dionysiou, New insights into the mechanism of visible light photocatalysis, J. Phys. Chem. Lett. 5 (2014) 2543–2554.

[10] T. Cottineau, A. Rouet, V. Fernandez, L. Brohana, M. Richard-Plouet, Intermediate band in the gap of photosensitive hybrid gel based on titanium oxide: role of coordinated ligands during photoreduction, J. Mater. Chem. A 2 (2014) 11499.

[11] S. Sun, X. Chang, X. Li, Z. Li, Synthesis of N-doped ZnO nanoparticles with improved photocatalytical activity, Ceram. Int. 39 (2013) 5197–5203.

[12] Y. Qiu, M. Yang, H. Fan, Y. Xu, Y. Shao, X. Yang, S. Yang, Synthesis and characterization of nitrogen doped ZnO tetrapods and application in photocatalytic degradation of organic pollutants under visible light, Mater. Lett. 99 (2013) 105–107.

[13] K. Siuzdak, M. Szkoda, M. Sawczak, A. Lisowska-Oleksiak, Novel nitrogen precursors for electrochemically driven doping of titania nanotubes exhibiting enhanced photoactivity, New J. Chem. 39 (2015) 2741–2751.

[14] V. Gombac, L. De Rogatis, A. Gasparotto, G. Vicario, T. Montini, D. Barreca, G. Balducci, P. Fornasiero, E. Tondello, M. Graziani, TiO_2 nanopowders doped with boron and nitrogen for photocatalytic applications, Chem. Phys. 339 (2007) 111–123.

[15] T. Cottineau, N. Béalu, P.-A. Gross, S.N. Pronkin, N. Keller, E.R. Savinova, V. Keller, One step synthesis of niobium doped titania nanotube arrays to form (N,Nb) co-doped TiO_2 with high visible light photoelectrochemical activity, J. Mater. Chem. A 1 (2013) 2151.

[16] Y. Zheng, L. Zheng, Y. Zhan, X. Lin, Q. Zheng, K. Wei, Ag/ZnO heterostructure nanocrystals: synthesis, characterization, and photocatalysis, Inorg. Chem. 46 (2007) 6980–6986.

[17] A. Bumajdad, M. Madkour, Understanding the superior photocatalytic activity of noble metals modified titania under UV and visible light irradiation, Phys. Chem. Chem. Phys. 16 (2014) 7146–7158.

[18] P. Cheng, C. Shao, X. Li, M. Zhang, X. Zhang, Y. Sun, Y. Liu, In situ assembly of well-dispersed Au nanoparticles on TiO_2/ZnO nanofibers: a three-way synergistic heterostructure with enhanced photocatalytic activity, J. Hazard. Mater. 237 (2012) 331–338.

[19] L. Li, X. Zhang, W. Zhang, L. Wang, X. Chen, Y. Gao, Microwave-assisted synthesis of nanocomposite Ag/ZnO-TiO2 and photocatalytic degradation Rhodamine B with different modes, Colloid Surf. A 457 (2014) 134–141.

[20] H. Zeng, P. Liu, W. Cai, S. Yang, X. Xu, Controllable Pt/ZnO porous nanocages with improved photocatalytic activity, J. Phys. Chem. C 112 (2008) 19620–19624.

[21] T. Gao, Q. Li, T. Wang, Sonochemical synthesis, optical properties, and electrical properties of core/shell-type ZnO Nanorod/CdS nanoparticle composite, Chem. Mater. 17 (2005) 887–892.

[22] M. Volokh, M. Diab, O. Magen, I. Jen-La Plante, K. Flomin, P. Rukenstein, N. Tessler, T. Mokari, Coating and enhanced photocurrent of vertically aligned zinc oxide nanowire arrays with metal sulfide materials, ACS Appl. Mater. Interfaces 6 (2014) 13594–13599.

[23] I. Robel, V. Subramanian, M. Kuno, P.V. Kamat, Quantum dot solar cells. harvesting light energy with CdSe nanocrystals molecularly linked to mesoscopic TiO_2 films, J. Am. Chem. Soc. 128 (2006) 2385–2393.

[24] J. Luo, L. Ma, T. He, T.F. Ng, S. Wang, H. Sun, H.J. Fan, TiO_2/(CdS, CdSe, CdSeS) nanorod heterostructures and photoelectrochemical properties, J. Phys. Chem. C 16 (2012) 11956–11963.

[25] M. Dahl, Y. Liu, Y. Yin, Composite titanium dioxide nanomaterials, Chem. Rev. 114 (2014) 9853–9889.

[26] R. Marschall, Semiconductor composites: strategies for enhancing charge carrier separation to improve photocatalytic activity, Adv. Funct. Mater. 24 (2014) 2421–2440.

[27] D.R. Miller, S.A. Akbar, P.A. Morris, Nanoscale metal oxide-based heterojunctions for gas sensing: a review, Sensor. Actuator. B 204 (2014) 250–272.

[28] F.-X. Xiao, Construction of highly ordered ZnO-TiO2 nanotube arrays (ZnO/TNTs) heterostructure for photocatalytic application, ACS Appl. Mater. Interfaces 4 (2012) 7055–7063.

[29] B.S. Shaheen, H.G. Salem, M.A. El-Sayed, N.K. Allam, Thermal/electrochemical growth and characterization of one-dimensional ZnO/TiO_2 hybrid nanoelectrodes for solar fuel production, J. Phys. Chem. C 117 (2013) 18502–18509.

[30] J.Y. Park, S.-W. Choi, J.-W. Lee, C. Lee, S.S. Kim, Synthesis and gas sensing properties of TiO2–ZnO core-shell nanofibers, J. Am. Ceram. Soc. 92 (2009) 2551–2554.

[31] J. Chang, Y. Kuga, I. Mora-Seró, T. Toyoda, Y. Ogomi, S. Hayase, J. Bisquert, Q. Shen, High reduction of interfacial charge recombination in colloidal quantum dot solar cells by metal oxide surface passivation, Nanoscale 7 (2015) 5446–5456.

[32] D. Shao, H. Sun, G. Xin, J. Lian, S. Sawyer, High quality ZnO–TiO2 core–shell nanowires for efficient ultraviolet sensing, Appl. Surf. Sci. 314 (2014) 872–876.

[33] F. Wang, J.-H. Seo, Z. Li, A.V. Kvit, Z. Ma, X. Wang, Cl-doped ZnO nanowires with metallic conductivity and their application for high-performance photoelectrochemical electrodes, ACS Appl. Mater. Interfaces 6 (2014) 1288–1293.

[34] N. Haghighia, Y. Abdia, F. Haghighib, Light-induced antifungal activity of TiO2 nanoparticles/ZnO nanowires, Appl. Surf. Sci. 257 (2011) 10096–10100.
[35] A.K. Chandiran, M. Abdi-Jalebi, M.K. Nazeeruddin, M. Grätzel, Analysis of electron transfer properties of ZnO and TiO2 photoanodes for dye-sensitized solar cells, ASC Nano 8 (3) (2014) 2261–2268.
[36] L.E. Greene, M. Law, B.D. Yuhas, P. Yang, ZnO-TiO2 Core-shell nanorod/P3HT solar cells, J. Phys. Chem. C 111 (5) (2007) 18451–18456.
[37] M. Law, L.E. Greene, A. Radenovic, T. Kuykendall, J. Liphardt, P. Yang, ZnO-Al2O3 and ZnO-TiO2 core-shell nanowire dye-sensitized solar cells, J. Phys. Chem. B 110 (2006) 22652–22663.
[38] O.V. Williams, N.C. Jeong, C. Prasittichai, O.K. Farha, M.J. Pellin, J.T. Hupp, Fast transporting ZnOTiO2 coaxial photoanodes for dye-sensitized solar cells based on ALD-modified SiO2 aerogel frameworks, ASC Nano 7 (6) (2012) 6185–6196.
[39] A. Katoch, J.-H. Kim, S.S. Kim, TiO2/ZnO inner/outer double-layer hollow fibers for improved detection of reducing gases, ACS Appl. Mater. Interfaces 6 (2014) 21494–21499.
[40] M. Wang, C. Huang, Y. Cao, Q. Yu, W. Guo, Q. Liu, J. Liang, M.A. Hong, A plasma sputtering decoration route to producing thickness-tunable ZnO/TiO2 core/shell nanorod arrays, Nanotechnology 20 (2009) 285311.
[41] J. Qiu, W. Yu, X. Gao, X. Li, Sol–gel assisted ZnO nanorod array template to synthesize TiO2 nanotube arrays, Nanotechnology 17 (2006) 4695–4698.
[42] S. Yuan, J. Mu, R. Mao, Y. Li, Q. Zhang, H. Wang, All-nanoparticle self-assembly ZnO/TiO2 heterojunction thin films with remarkably enhanced photoelectrochemical activity, ACS Appl. Mater. Interfaces 6 (2014) 5719–5725.
[43] T.J. Athauda, J.G. Neff, L. Sutherlin, U. Butt, R.R. Ozer, Systematic study of the structure-property relationships of branched hierarchical TiO2/ZnO nanostructures, ACS Appl. Mater. Interfaces 4 (2012) 6917–6926.
[44] X. Zheng, D. Li, X. Li, J. Chen, C. Cao, J. Fang, J. Wang, Y. He, Y. Zheng, Construction of ZnO/TiO2 photonic crystal heterostructures for enhanced photocatalytic properties, Appl. Catal. B-Environ. 168 (2015) 408–415.
[45] G.K.L. Goh, H.Q. Le, T.J. Huang, B.T.T. Hui, Low temperature grown ZnO@TiO2 core shell nanorod arrays for dye sensitized solar cell application, J. Solid State Chem. 214 (2014) 17–23.
[46] V. Manthina, J.P. Correa Baena, G. Liu, A.G. Agrios, ZnO-TiO2 nanocomposite films for high light harvesting efficiency and fast electron transport in dye-sensitized solar cells, J. Phys. Chem. C 116 (2012) 23864–23870.
[47] S. Hernandez, V. Cauda, A. Chiodoni, S. Dallorto, A. Sacco, D. Hidalgo, E. Celasco, C.F. Pirri, Optimization of 1D ZnO@TiO2 core-shell nanostructures for enhanced photoelectrochemical water splitting under solar light illumination, ACS Appl. Mater. Interfaces 6 (15) (2014) 12153–12167.
[48] K. Pan, Y. Dong, W. Zhou, Q. Pan, Y. Xie, T. Xie, G. Tian, G. Wang, Facile fabrication of hierarchical TiO2 nanobelt/ZnO nanorod heterogeneous nanostructure: an efficient photoanode for water splitting, ACS Appl. Mater. Interfaces 5 (2013) 8314–8320.
[49] L. Wang, S. Liu, Z. Wang, Y. Zhou, Y. Qin, Z.L. Wang, Piezotronic effect enhanced photocatalysis in strained anisotropic ZnO/TiO2 nanoplatelets via thermal stress, ACS Nano 10 (2) (2016) 2636–2643.
[50] M. Kwiatkowski, I. Bezverkhyy, M. Skompska, ZnO nanorods covered with a TiO2 layer: simple sol–gel preparation, and optical, photocatalytic and photoelectrochemical properties, J. Mater. Chem A 3 (2015) 12748–12760.
[51] K. Zarębska, M. Kwiatkowski, M. Gniadek, M. Skompska, Electrodeposition of Zn(OH)2, ZnO thin films and nanosheet-like Zn seed layers and influence of their morphology on the growth of ZnO nanorods, Electrochim. Acta 98 (2013) 255–262.
[52] ISO 10678-2010.
[53] A. Sarkar, A.K. Singh, G.G. Khan, D. Sarkar, K. Mandal, TiO2/ZnO core/shell nano-heterostructure arrays as photo-electrodes with enhanced visible light photoelectrochemical performance, RSC Adv. 4 (2014) 55629.
[54] J. Tauc, Optical properties and electronic structure of amorphous Ge and Si, Mater. Res. Bull. 3 (1968) 37–46.
[55] D. Monllor-Satoca, R. Gómez, Electrochemical method for studying the kinetics of electron recombination and transfer reactions in heterogeneous photocatalysis: the effect of fluorination on TiO2 nanoporous layers, J. Phys. Chem. C 112 (2008) 139–147.
[56] L. Straka, Y. Yagodzinskyy, H. Kawakami, J. Romu, R. Ilola, H. Hänninen, Open-circuit potential as an indicator of damage of atomic layer deposited TiO2 on AISI 304 stainless steel, Thin Solid Films 517 (2008) 641–647.
[57] M. Quintana, T. Edvinsson, A. Hagfeldt, G. Boschloo, Comparison of dye-sensitized ZnO and TiO2 solar cells: studies of charge transport and carrier lifetime, J. Phys. Chem. C 11 (2007) 1035–1041.
[58] A. Zaban, M. Greenshtein, J. Bisquert, Determination of the electron lifetime in nanocrystalline dye solar cells by photovoltage decay measurements, J. ChemPhysChem 4 (2003) 859–864.
[59] A. Fujishima, X. Zhang, D.A. Tryk, TiO2 photocatalysis and related surface phenomena, Surf. Sci. Rep. 63 (2008) 515–582.
[60] T. Bak, W. Li, J. Nowotny, A.J. Atanacio, J. Davis, Photocatalytic properties of TiO2: evidence of the key role of surface active sites in water oxidation, J. Phys. Chem. A 119 (2015) 9465–9473.
[61] A.D. Smigelskas, E.O. Kirkendall, Zinc diffusion in alpha brass, Trans. AIME 171 (1947) 130–142.
[62] E.O. Kirkendall, Diffusion of zinc in alpha brass, Trans. AIME 147 (1942) 104–110.
[63] E.O. Kirkendall, L. Thomassen, C. Upthegrove, Rates of diffusion of copper and zinc in alpha brass, Trans. AIME 133 (1939) 186–203.
[64] H.J. Fan, U. Gösele, M. Zacharias, Formation of nanotubes and hollow nanoparticles based on kirkendall and diffusion processes: a review, Small 3 (10) (2007) 1660–1671.
[65] B. Schumacher, V. Plzak, J. Cai, R.J. Behm, Reproducibility of highly active Au/TiO2 catalyst preparation and conditioning, Catal. Lett. 101 (2005) 215–224.
[66] H.M. Liu, W.S. Yang, Y. Ma, Y. Cao, N.J. Yao, J. Zhang, T.D. Hu, Synthesis and characterization of titania prepared by using a photoassisted sol-gel method, Langmuir 19 (2003) 3001–3005.
[67] Y. Lei, L.D. Zhang, G.W. Meng, G.H. Li, X.Y. Zhang, C.H. Liang, W. Chen, S.X. Wang, Preparation and photoluminescence of highly ordered TiO2 nanowire arrays, Appl. Phys. Lett. 78 (2001) 1125–1127.
[68] F.J. Knorr, J.L. McHale, Spectroelectrochemical photoluminescence of trap states of nanocrystalline TiO2 in aqueous media, J. Phys. Chem. C 117 (2013) 13654–13662.
[69] J. Shi, J. Chen, Z. Feng, T. Chen, Y. Lian, X. Wang, C. Li, Photoluminescence characteristics of TiO2 and their relationship to the photoassisted reaction of water/methanol mixture, J. Phys. Chem. C 111 (2007) 693–699.
[70] X. Pan, M.-Q. Yang, X. Fu, N. Zhang, Y.-J. Xu, Defective TiO2 with oxygen vacancies: synthesis, properties and photocatalytic applications, Nanoscale 5 (2013) 3601–3614.
[71] Y. Yang, R. Scholz, H.J. Fan, D. Hesse, U. Gösele, M. Zacharias, Multitwinned spinel nanowires by assembly of nanobricks via oriented attachment: a case study of Zn2TiO4, ASC Nano 3 (3) (2009) 555–562.